Miyagi T, Shiotani B, Miyoshi R, Yamamoto T, Oka T, Umezawa K, Ochiya T, Takano M, Tahara H.	DSE-FRET: A new anticancer drug screening assay for DNA binding proteins.	Cancer Sci	105	870-874	2014
Shimamoto A, Kagawa H, Zensho K, Sera Y, Kazuki Y, Osaki M, Oshimura M, Ishigaki Y, Hamasaki K, Kodama Y, Yuasa S, Fukuda K, Hirashima K, Seimiya H, Koyama H, Shimizu T, Takemoto M, Yokote K, Goto M, Tahara H.	Reprogramming suppresses premature senescence phenotypes of Werner syndrome cells and maintains chromosomal stability over long-term culture.	PLoS One.	9	e112900	2014
Yamasaki S, Taguchi Y, Shimamoto A, Mukasa H, Tahara H, Okamoto T.	Generation of human induced pluripotent stem (iPS) cells in serum- and feeder-free defined culture and TGF-Beta1 regulation of pluripotency.	PLoS One	9	e87151	2014
Yuyama K, Sun H, Sakai S, Mitsutake S, Okada M, Tahara H, Furukawa J, Fujitani N, Shinohara Y, Igarashi Y.	Decreased amyloid-β pathologies by intracerebral loading of glycosphingolipid-enriched exosomes in Alzheimer model mice.	J Biol Chem.	289	24488-24498	2014
Li XJ, Goodwin CB, Nabinger SC, Richine BM, Yang Z, Hanenberg H, Ohnishi H, Matozaki T, Feng GS, Chan RJ.	Protein-tyrosine Phosphatase Shp2 Positively Regulates Macrophage Oxidative Burst.	J Biol Chem.	290(7)	3894-3909	2015
Koshimizu H, Takao K, Matozaki T, Ohnishi H, Miyakawa T.	Comprehensive behavioral analysis of cluster of differentiation 47 knockout mice	PLoS One.	9(2)	e89584	2014
Murata Y, Kotani T, Ohnishi H, Matozaki T.	The CD47-SIRPα signalling system: its physiological roles and therapeutic application.	J Biochem.	155(6)	335-344	2014
Stenberg Å, Karlsson A, Feuk-Lagerstedt E, Christenson K, Bylund J, Oldenborg A, Vesterlund L, Matozaki T, Sehlin J, Oldenborg PA.	Signal regulatory protein alpha is present in several neutrophil granule populations and is rapidly mobilized to the cell surface to negatively fine-tune neutrophil accumulation in inflammation.	J Innate Immun.	6(4)	553-560	2014

Yamashita H, Kotani T, Park JH, Murata Y, Okazawa H, Ohnishi H, Ku Y, Matozaki T.	Role of the protein tyrosine phosphatase Shp2 in homeostasis of the intestinal epithelium.	PLoS One.	9(3)	e92904	2014
Dansako H , Hiramoto H, Ikeda M, Wakita T, Kato N.	Rab18 is required for viral assembly of hepatitis C virus through trafficking of the core protein to lipid droplets.	Virology	462-463	166-174	2014
Hara Y, Yanatori I, Ikeda M, Kiyokage E, Nishina S, Tomiyama Y, Toida K, Kishi F, Kato N, Imamura M, Chayama K, Hino K.	Hepatitis C virus core protein suppresses mitophagy by interacting with Parkin in the context of mitochondrial depolarization.	American Journal of Pathology	184(11)	3026-3039	2014
Kato N , Sejima H, Ueda Y, Mori K, Satoh S, Dansako H, Ikeda M.	Genetic characterization of hepatitis C virus in long-term RNA replication using Li23 cell culture systems.	PLoS ONE	9(3)	e91156	2014
Matsuda M, Suzuki R, Kataoka C, Watashi K, Aizaki H, Kato N, Matsuura Y, Suzuki T, Wakita T.	Alternative endocytosis pathway for productive entry of hepatitis C virus.	Journal of General Virology	95(12)	2658-2667	2014
Matsuno K , Ueda Y, Fukuda M, Onoda K, Waki M, Ikeda M, Kato N, Miyachi H.	Synthesis and inhibitory activity on hepatitis C virus RNA replication of 4-(1,1,1,3,3,3-hexafluoro-2-hydroxy-2-propyl)aniline analogs.	Bioorganic & Medicinal Chemistry Letters	27(17)	4276-4280	2014
Okamoto M, Oshiumi H, Azuma M, Kato N, Matsumoto M, Seya T.	IPS-1 is essential for type III interferon production by hepatocytes and dendritic cells in response to hepatitis C virus infection.	Journal of Immunology	192(6)	2770-2777	2014
Shimada H, Haraguchi K, Hotta K, Miyaike T, Kitagawa Y, Tanaka H, Kaneda R, Abe H, Shuto S, Mori K, Ueda Y, Kato N, Snoeck R, Andrei G, Balzarini J.	Synthesis of 3',4'-difluoro-3'-deoxyribonucleosides and its evaluation of the biological activities: Discovery of a novel type of anti-HCV agent 3',4'-difluorocordycepin.	Bioorganic & Medicinal Chemistry	22(21)	6174-6182	2014
Ueda Y, Mori K, Satoh S, Dansako H, Ikeda M, Kato N.	Anti-HCV activity of the Chinese medicinal fungus *Cordyceps militaris*.	Biochemical and Biophysical Research Communications	447	341-345	2014

Ⅳ. 研究成果の刊行物・別刷

Hepatology Research

Hepatology Research 2015; **45**: 470–479 doi: 10.1111/hepr.12364

Original Article

Intrahepatic triglyceride measurement and estimation of viability in rat fatty livers by near-infrared spectroscopy

Yasuhiro Fudaba, Akihiko Oshita, Hirotaka Tashiro and Hideki Ohdan

Department of Surgery, Division of Frontier Medical Science, Graduate School of Biomedical Sciences, Hiroshima University, Hiroshima, Japan

Aim: This study investigated the features of fatty livers using near-infrared (NIR) spectroscopy and validated the usefulness of NIR spectroscopy for the measurement of intrahepatic triglyceride (TG) contents and evaluation of viability in fatty livers.

Methods: *In vitro*, we examined specific spectra for each purified TG fraction by NIR. *In vivo*, the differences between the spectra obtained from normal and fatty livers before warm ischemia and the differences between the spectra obtained from each rat liver before and after warm ischemia were subjected to multicomponent analysis.

Results: *In vitro* experiments revealed a specific peak at 925 nm in major TG fractions, and NIR spectroscopy precisely detected changes in TG volume. *In vivo* experiments revealed that NIR spectroscopy detected TG content changes in rat fatty livers induced by a choline-deficient diet following the addition of purified TG spectrum for NIR spectroscopic analysis in least square curve fitting. The TG level in the fatty livers measured by NIR spectroscopy significantly correlated with the morphometric measurement of lipid content in the livers. NIR spectroscopy also revealed decreased levels of total hemoglobin (Hb) and oxidized Hb and maintenance of homeostasis in cytochrome redox states in fatty livers under normal condition. However, NIR spectroscopy showed irreversible deterioration of hepatic microcirculation, Hb oxygenation and homeostasis of the cytochrome redox states in fatty livers after 60-min warm ischemia reperfusion.

Conclusion: These studies demonstrated that NIR spectroscopy can quantitatively measure the intrahepatic TG content in addition to simultaneously evaluating microcirculation and Hb oxygenation.

Key words: fatty liver, ischemia–reperfusion injury, liver transplantation, near-infrared spectroscopy, primary graft dysfunction

INTRODUCTION

IT IS WELL known that donor livers with severe fatty infiltration are frequently associated with primary graft non-function after transplantation.[1–3] Many reports indicated that sinusoidal microcirculatory disturbance in fatty liver was the major cause of primary graft non-function.[4–8] Therefore, most fatty livers have been discarded without appropriate estimation. However, some reports show that the incidence of primary graft non-function with mild fatty liver is not statistically different compared to that with non-fatty liver.[1,9,10] Precise estimation of fatty liver before implantation may not only prevent the occurrence of primary graft non-function but also salvage marginal donor livers. Presently, the diagnosis of fatty liver is made clinically by ultrasound tomography or computed tomography, which can be very useful for diagnosing cases of typical fatty liver. However, these methods are not satisfactory for grading fatty infiltration or estimating the viability of the fatty liver. Liver biopsy is also reportedly useful for detecting and grading fatty infiltration.[1,11,12] However, an invasive procedure is not suitable for the transplantation situation, and a single-point liver biopsy may not be representative of the whole liver. Although magnetic

Correspondence: Dr Hideki Ohdan, Department of Surgery, Division of Frontier Medical Science, Graduate School of Biomedical Sciences, Hiroshima University, 1-2-3 Kasumi, Minami-ku, Hiroshima 734-8551, Japan. Email: hohdan@hiroshima-u.ac.jp

Author contribution: The first two authors contributed equally to this work. Study design was performed by Hirotaka Tashiro and Hideki Ohdan; acquisition of data by Yasuhiro Fudaba; analysis and interpretation by Yasuhiro Fudaba and Hideki Ohdan; manuscript drafting by Yasuhiro Fudaba and Akihiko Oshita; revision by Akihiko Oshita; and statistical advice by Hirotaka Tashiro and Hideki Ohdan.

Received 16 February 2014; revision 15 May 2014; accepted 16 May 2014.

resonance spectroscopy (MRS) was recently reported as useful for measuring the hepatic triglyceride (TG) content,[13–15] MRS is relatively expensive and has poor portability.

Near-infrared (NIR) spectroscopy was first introduced by Jobsis in 1977.[16] A significant amount of radiation can be effectively transmitted through biological materials over long distances in the 700–1300 nm range of NIR light. Because the absorption intensity of NIR light depends on the level of hemoglobin (Hb) oxygenation, the redox state of cytochrome aa_3 (Cyt. aa_3) and biological content, NIR spectroscopy is currently being applied in the medical field to evaluate oxygen availability and oxygen consumption relationships within living tissues such as brain, muscle, lung and liver.[17–25] We previously reported that *in vivo* NIR spectroscopy non-invasively measured the tissue Hb oxygenation, the redox state of Cyt. aa_3 and water content, and could additionally evaluate the viability of grafts damaged by warm ischemia in the living rat liver and lung. However, NIR spectroscopic evaluation for diseased liver such as fatty liver has not been reported. Theoretically, NIR spectroscopy has the potential to measure not only the level of Hb oxygenation, the redox state of Cyt. aa_3 and water, but also the fat component by addition of a purified fat spectrum to the standard spectra of the biological components for curve fitting in multicomponent analysis.

In the present study, we demonstrated the potential of using NIR spectroscopy for detecting and grading hepatic fatty infiltration simultaneous to estimating viability.

METHODS

NIR spectroscopic detection of standard spectra for fat content *in vitro*

A DETAILED REPORT has described the contents of fat that accumulates in the livers by the choline-deficient diet (CDD).[10] According to this report, TG are the main content of the accumulated fat and consist mainly of the following six fragments: (i) trilinolein; (ii) triolein; (iii) tripalmitin; (iv) triarachidin; (v) tristearin; and (vi) tripalmitolein. To directly investigate the ability of NIR spectroscopy to detect changes in fat volume, we examined specific spectra for each purified TG fraction (Sigma, Tokyo, Japan) and further investigated changes in the spectra by serial dilution with chloroform.

A multichannel photometer (MCPD-2000; Otsuka Electrical, Osaka, Japan) with quartz optical fibers and a 300-W halogen lamp, as the light source, was used to observe spectra for each TG fraction. The tips of the optical fibers were fixed for a crystal cuvette with a sample. The absorbance was scanned within the 500–1100 nm range, and the sampling time of each scan was 200 msec. The spectra from a series of 20 scans were averaged using a personal computer (PC-9801 Xs; NEC, Tokyo, Japan).

Animals

Male inbred Lewis rats were obtained from Charles River (Kyoto, Japan). The animals weighed 180–250 g each and were housed in conventional animal facilities with 12-h intervals of light and darkness in a room maintained at 24°C. The animals were allowed free access to water. To induce fatty changes in the rat livers, some rats were fed a CDD (Oriental Yeast, Kyoto, Japan) for 1, 3 or 7 weeks. With this model fed a CDD, TG is the main constituent of the fatty deposits.[10] The control rats were fed standard laboratory chow. All surgical procedures were performed under ether anesthesia, and all animal experiments were performed according to the guidelines set by the National Institutes of Health (NIH publication no. 85-23, revised 1985).

In vivo NIR spectroscopy and measurement of 60 min of hepatic warm ischemia–reperfusion injury

The same instruments applied for the *in vitro* studies were used for *in vivo* NIR spectroscopy. After performing a laparotomy, the tips of the fiber bundles for NIR spectroscopy (the distance between the bundles was 3 mm) were fixed at a position approximately 3 mm above the left lobe of the liver, and the NIR spectrum before ischemia was obtained. We then performed a 60-min warm ischemia of the left hepatic lobe by clamping the left portal vein and left hepatic artery with a microvascular clip. After releasing the clip, NIR spectroscopic measurements were performed at 5-min intervals for 60 min. The differences between the spectra obtained from normal and fatty livers before warm ischemia were subjected to multicomponent analysis, and the differences between the spectra obtained from each rat liver before and after warm ischemia were also subjected to multicomponent analysis.

Histological examination and measurement of fatty areas

The non-ischemic right lobes of the livers were excised after completion of NIR spectroscopic measurement, and were fixed in 10% buffered formalin, embedded in paraffin, sectioned and stained with hematoxylin–eosin. The grade of fatty change for each specimen was deter-

mined by calculating the average percentage of the steatotic area in three fields in a blind manner after conversion to grayscale using image analysis so that all fat droplets were selected in contrast to the surrounding parenchymal and trial structure. The imaging analysis was performed using Adobe Photoshop version 6.0.

Statistical analysis

All data are shown as mean ± standard error of the mean, and the unpaired Student's *t*-test was used to calculate *P*-values. Regressions between variables were assessed by linear regression analysis. $P < 0.05$ was considered statistically significant. Statistical analysis was performed with Statview version 5.0 (SAS Institute, Cary, NC, USA).

RESULTS

Ability of NIR spectroscopy to determine the standard spectra for fat content *in vitro*

THE SPECTRA FOR each purified TG fraction shows that all of the spectra have a specific peak at 925 nm (Fig. 1). In addition, there was a significant correlation in each TG concentration with peak level, indicating the ability of NIR spectroscopy to quantify changes in TG content (Fig. 2).

Histology of CDD-induced fatty liver in rats

Liver specimens from control rats showed normal histological findings, and the calculated fatty area varied from 1.5% to 4.7%. Administration of CDD induced fatty infiltration in the liver of all rats, which was predominantly macrovesicular steatosis (Fig. 3). One-week administration of CDD induced mild fatty liver, and the calculated fatty area varied from 13.8% to 27.6%. In addition, 3- and 7-week administration of CDD induced moderate to severe fatty liver, and the calculated fatty area varied from 38.2% to 62.6% and from 37.3% to 50.4%, respectively. The sinusoidal lumens in 1-week-CDD rats were compressed, and more severe sinusoidal compressions were observed in 3- or 7-week-CDD rats.

In vivo NIR spectroscopic measurement before warm ischemia

The difference in the spectrum between standard normal liver and CDD-induced fatty liver was analyzed

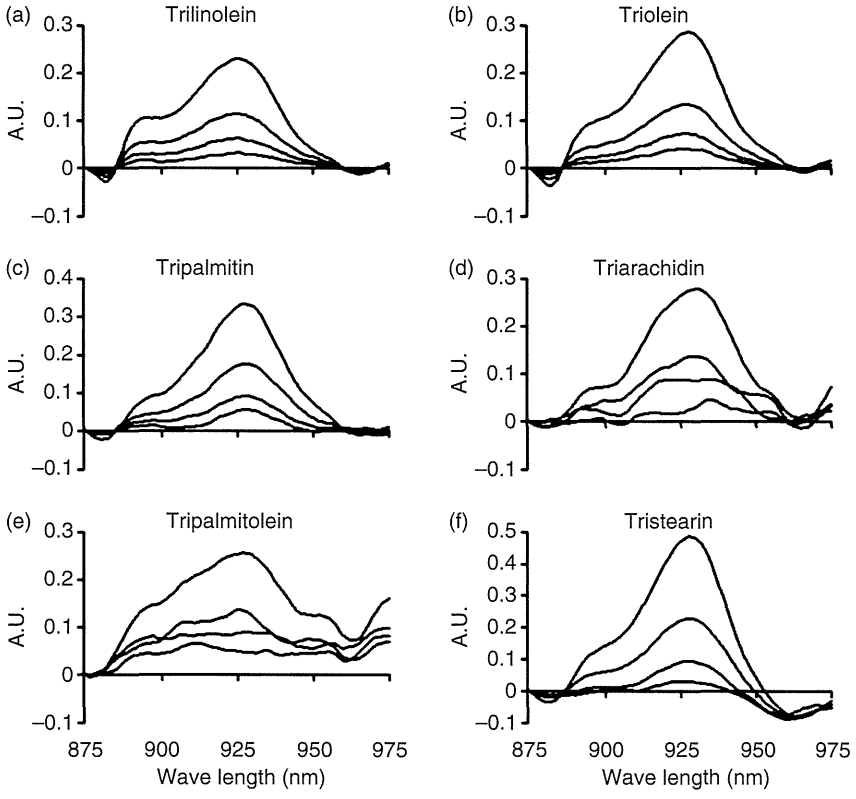

Figure 1 Absorption spectra of each triglyceride (TG) fraction at concentrations of 1.0, 0.5, 0.25 and 0.125. All spectra had a specific peak at 925 nm, and these peak values decreased in proportion to the concentration. (a) Trilinolein, (b) triolein, (c) tripalmitin, (d) triarachidin, (e) tripalmitolein, (f) tristearin. A.U., arbitrary unit.

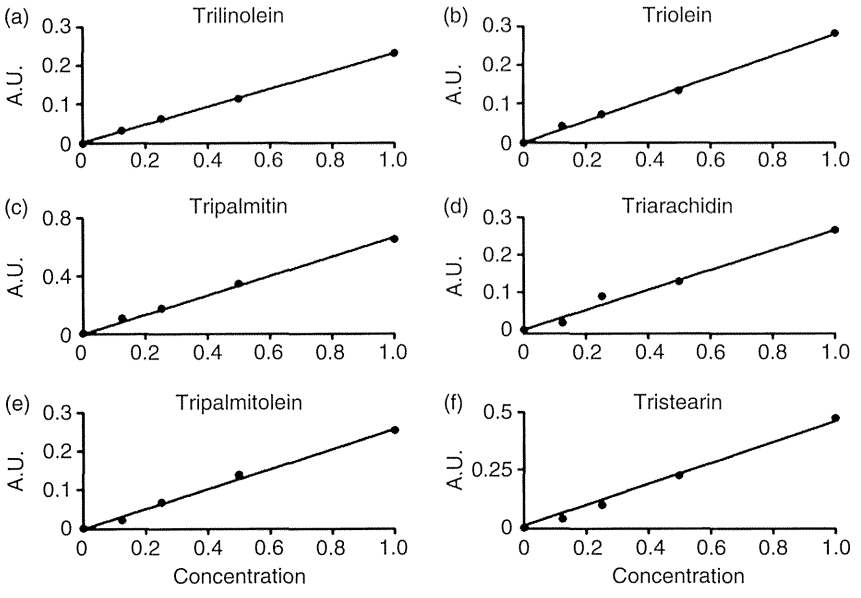

Figure 2 Linear correlations between changes at the peak of 925 nm in each triglyceride (TG) fraction measured by near-infrared (NIR) spectroscopy and the predetermined TG fraction concentration *in vitro*. A significant correlation was observed for each TG concentration. (a) Trilinolein ($P < 0.0001$), (b) triolein ($P < 0.0001$), (c) tripalmitin ($P < 0.0001$), (d) triarachidin ($P < 0.0001$), (e) tripalmitolein ($P < 0.0001$), (f) tristearin ($P < 0.0001$). A.U., arbitrary unit.

by a curve-fitting technique based on the least-square method within the 700–1000 nm range. In this analysis, we used the standard spectra of purified oxy-Hb, deoxy-Hb, oxidized-Cyt. aa_3, reduced-Cyt. aa_3 and water (Fig. 4). To investigate fat quantity, we added standard spectra of purified triolein as a representation of the fat component (Fig. 4). The six components were fitted with the following equation:

$$\begin{aligned} OD(\lambda) = L(\lambda)\cdot(e_1(\lambda)\bullet\Delta[\text{oxy-Hb}] + e_2(\lambda)\cdot\Delta[\text{deoxy-Hb}] \\ + e_3(\lambda)\cdot\Delta[\text{oxidized-Cyt. } aa_3] \\ + e_4(\lambda)\cdot\Delta[\text{reduced-Cyt. } aa_3] \\ + e_5(\lambda)\cdot\Delta[\text{triolein}] + e_6(\lambda)\cdot\Delta[\text{water}]) \end{aligned}$$

where $OD(\lambda)$, $L(\lambda)$ and $e_{1\text{-}6}(\lambda)$ are optical density, mean light path length and the extinction coefficient of each

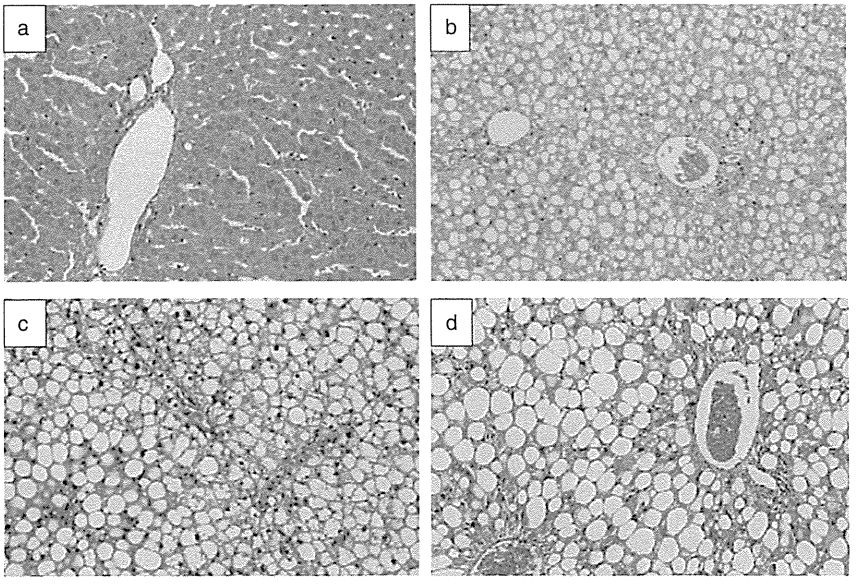

Figure 3 Light micrographs (hematoxylin–eosin, original magnification ×100) of liver specimens. (a) Normal liver, (b) 1-week-choline-deficient diet (CDD)-fed liver, (c) 3-week-CDD-fed liver, (d) 7-week-CDD-fed liver. All rats administrated CDD exhibited induced fatty infiltration in the liver, which was predominantly macrovesicular steatosis. The sinusoidal lumens in 1-week-CDD rats were compressed, and more severe sinusoidal compressions were observed in 3- or 7-week-CDD rats. The calculated fat areas for (a), (b), (c) and (d) were 1.52%, 26.16%, 38.17% and 43.0%, respectively.

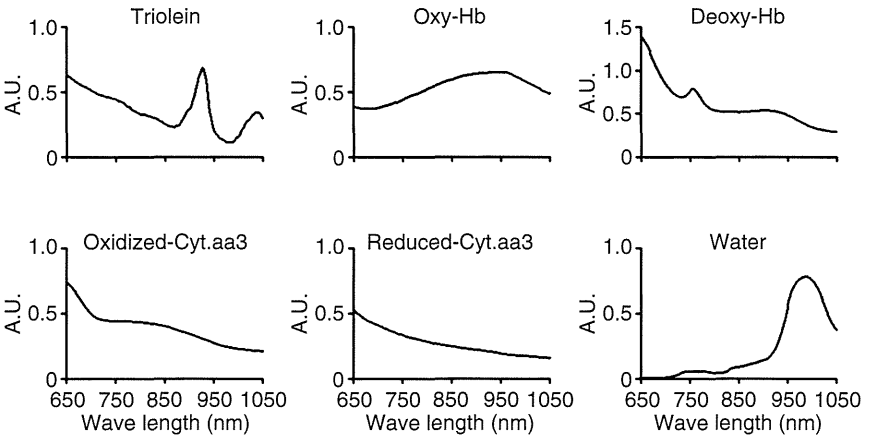

Figure 4 Absorption spectra used as standard spectra in the multicomponent analysis of near-infrared (NIR) spectroscopy. The spectrum of triolein has a strong and characteristic peak at approximately 925 nm. A.U., arbitrary unit.

component at a wavelength of λ, respectively. The relative changes in each component were detected using this multicomponent analysis calculated on the basis of singular value decomposition.

Figure 5 shows the levels in each parameter (total Hb, oxy-Hb, deoxy-Hb, oxidized-Cyt. aa_3, reduced-Cyt. aa_3 and TG) of NIR spectroscopy immediately after laparotomy in each group. NIR spectroscopic analysis for

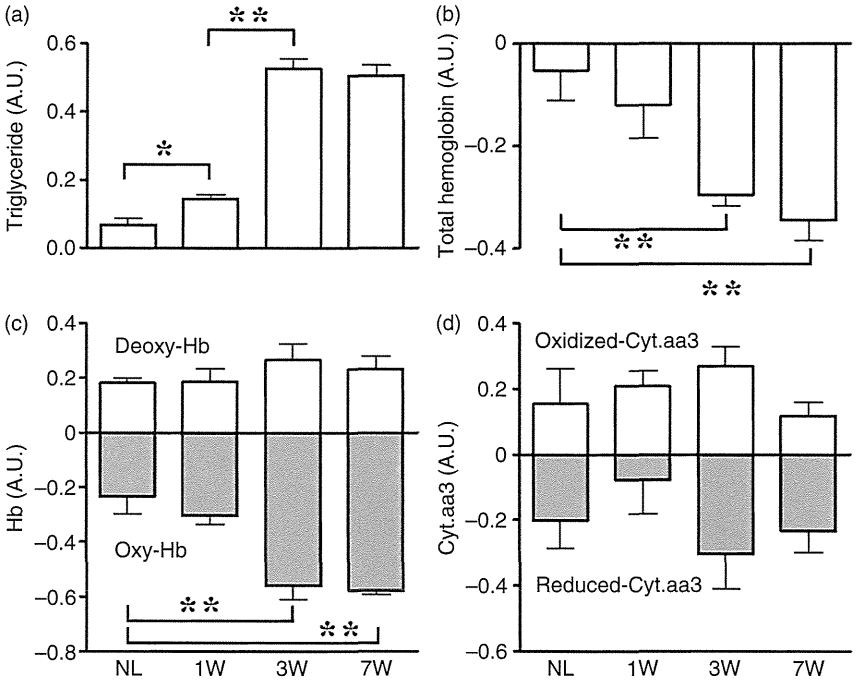

Figure 5 Levels of each parameter of near-infrared (NIR) spectroscopy immediately after laparotomy in each group. (a) Triglyceride (TG). NIR spectroscopic analysis for measuring TG in choline-deficient diet (CDD)-induced fatty livers detected significant differences compared to normal livers. (b) Total hemoglobin (Hb). Total Hb levels in 3- or 7-week-CDD rat livers were significantly decreased compared to those in normal livers. (c) Oxy-Hb (solid bar) and deoxy-Hb (open bar). Oxy-Hb levels in 3- or 7-week-CDD rat livers were significantly decreased compared to those in normal livers. (d) Oxidized-cytochrome aa_3 (Cyt. aa_3) (open bar) and reduced-Cyt. aa_3 (solid bar). There was no statistically significant different between the groups. 1W, 1-week-CDD fed rat group ($n = 6$); 3W, 3-week-CDD fed rat group ($n = 6$); 7W, 7-week-CDD fed rat group ($n = 6$); A.U., arbitrary unit; NL, normal diet fed rat group ($n = 4$). Results are expressed as mean ± standard error of the mean. $^*P < 0.05$, $^{**}P < 0.01$.

measuring TG in CDD-induced fatty livers detected significant differences compared to normal livers. However, the level of TG in 7-week-CDD livers was not significantly different compared to that in 3-week-CDD livers. These results indicate that the level of TG in CDD-induced fatty liver reached a maximum by 3 weeks and remained at a constant level after 3 weeks. Parameters other than TG were not significantly different between normal rat livers and 1-week-CDD livers. However, total Hb and oxy-Hb levels were significantly decreased in 3- or 7-week-CDD rat livers compared to those in normal rat livers. On the other hand, the levels of oxidized-Cyt. aa_3 and reduced-Cyt. aa_3 were not statistically different among each group. These findings indicate that mitochondrial cytochrome redox states were maintained in fatty livers under normal conditions despite hypoxia and microcirculatory disturbance.

Correlation between measurement of fatty liver by NIR spectroscopy and histological assessment

The relationship between TG level in each rat liver measured by NIR spectroscopy and histological examination for fatty change in each rat liver is shown in Figure 6, using 25 rat livers in total; four livers from standard-chow fed rats, six livers from 1-week-CDD fed rats, six livers from 3-week-CDD fed rats and nine livers from 7-week-CDD fed rats. This relationship exhibited a statistically significant positive linear correlation ($R = 0.92$, $P < 0.0001$).

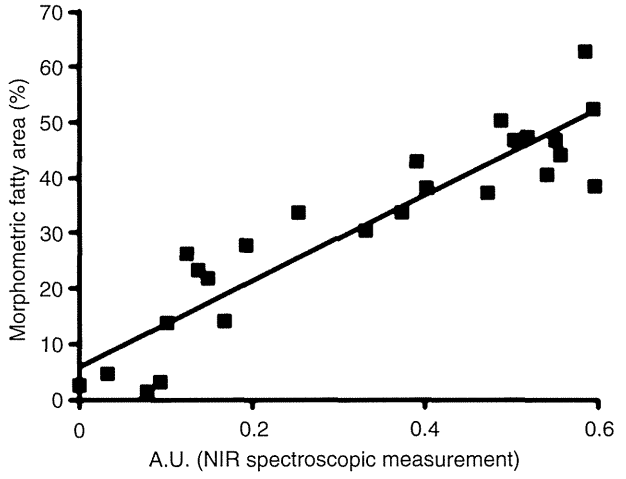

Figure 6 Correlation between triglyceride (TG) levels in rat livers measured by near-infrared (NIR) spectroscopy and by morphometric examination. These measurements exhibited a statistically significant positive linear correlation ($n = 25$, $R = 0.92$, $P < 0.0001$). A.U., arbitrary unit.

In vivo NIR spectroscopic measurement after 60 min of warm ischemia

The time courses of the relative changes of total Hb, oxy-Hb and deoxy-Hb after reperfusion in the livers are shown in Figure 7. In normal livers, these parameters showed minimum changes and immediately recovered to the pre-ischemic level after 60 min of reperfusion. However, the relative changes of total Hb and deoxy-Hb in the livers of 3-week-CDD rats after reperfusion were highly elevated and consistently remained at a high level during observation, whereas these parameters in 1-week-CDD rats gradually recovered to the pre-ischemic level. The time course of oxy-Hb in the livers of 3-week-CDD rats after reperfusion also showed slow recovery compared to that of 1-week-CDD rats. The time courses of the relative changes of oxidized-Cyt. aa_3 and reduced-Cyt. aa_3 in the livers after reperfusion are shown Figure 7. These parameters remained close to the pre-ischemic level in the normal livers after ischemia–reperfusion. In contrast, relative changes of oxidized-Cyt. aa_3 and reduced-Cyt. aa_3 in fatty livers after ischemia–reperfusion did not return to the level of pre-ischemia.

DISCUSSION

THE NIR SPECTROSCOPIC technique is widely accepted and applied in many fields to evaluate the content of various materials, and this technique has been used in the fields of medicine and food industry at the wavelength range 1000–2500 nm for detecting fat content in milk and feces.[26,27] However, NIR spectroscopic evaluation for detecting fat content in a living organ has not been established. Moreover, at 1000–2500 nm, there are little simultaneous advantages to evaluate other biological components in living organs such as oxy-Hb, deoxy-Hb, oxidized-Cyt. aa_3, reduced-Cyt. aa_3 and water, because these components have characteristic spectra at 600–1300 nm. In this study, we developed an NIR spectroscopic technique that showed the potential for evaluating the intrahepatic fat content simultaneously with liver viability.

Fatty liver is a relatively asymptomatic disease. The incidence of fatty livers among potential donor livers is unexpectedly high and reportedly ranges 15–24% in autopsies after accidental death.[28–30] In the transplantation field, donor livers with severe fatty infiltration are

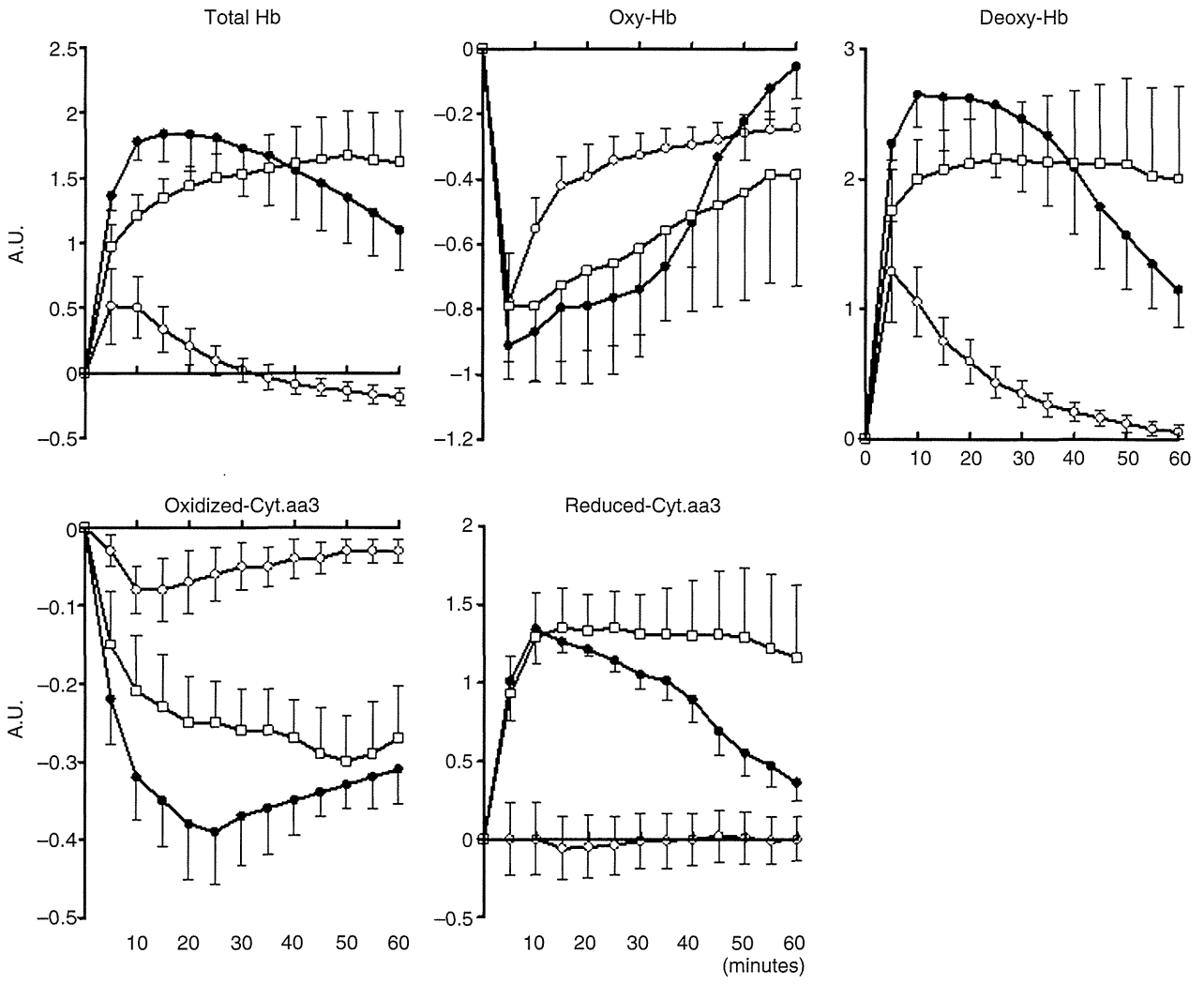

Figure 7 Time course changes of each parameter in rat liver after 60 min of warm ischemia. Open circles, normal rat liver group ($n = 4$); closed circles, 1-week-choline-deficient diet (CDD) fed rat liver group ($n = 5$); open squares, 3-week-CDD fed rat liver group ($n = 5$). Results are expressed as mean ± standard error of the mean; error bars not shown appear within the data points. A.U., arbitrary unit.

generally considered to be at high risk for primary graft non-function (PNF),[4–7] and fatty livers are usually discarded to decrease the risk of PNF for this reason. However, some institutions have reported successful transplantation of fatty livers, suggesting that transplantation of a fatty liver does not always result in a primary non-functioning graft.[1,9,11,31] Presently, there is no established method for precisely evaluating the viability of fatty livers. Therefore, establishing such an evaluation method for fatty livers could potentially increase the number of marginal donor sources.

It is well known that the main constituent of fatty droplets deposited in fatty livers is TG. In addition, TG content in fatty liver was reported to constitute from some fractions.[10] Our detailed *in vitro* investigation revealed that each purified TG fraction had a strong and characteristic peak at 925 nm, and NIR spectroscopy precisely detected changes in the TG fraction volume (Figs 1,2). In addition, the spectra of purified TG fractions were different from any of the biological pigments in the NIR region (Fig. 4). Among the TG fractions, triolein was reported to constitute the main fraction and correlate well with total TG volume.[10] Therefore, we selected the triolein spectrum as the representative of the TG component in NIR spectroscopy analysis, and assumed that it could serve as a useful parameter for

measuring the fat content in the liver as well as measuring liver oxygenation and the cytochrome redox state.

In this study, we applied NIR spectroscopy to CDD-induced fatty livers to evaluate the possibility of using *in vivo* NIR spectroscopy to quantify hepatic TG content. Histological findings revealed the development of mild-to-moderate fatty changes in the livers of rats that were administrated CDD for 1 week (Fig. 3). On the other hand, we found moderate-to-severe fatty changes in the livers of rats that were administrated CDD for 3 or 7 weeks. In order to histologically evaluate the precise degree of fatty liver, we calculated the fat area using the fixed specimens. We observed a significant correlation in the relationship between the fat content calculated by NIR spectroscopy and the morphometric measurement (Fig. 6). Kitai *et al.* also reported the possibility of quantifying the fatty changes in the rat liver by NIR time-resolved spectroscopy using the optical absorption and reduced scattering coefficients,[32] but this method can quantify the fat content only in a perfused liver. However, our NIR spectroscopic technique could detect fat content in the liver in any condition with high specificity and sensitivity, because we analyzed the data using the specific spectrum for TG.

The *in vivo* studies presented herein show the ability of NIR spectroscopy to reveal the features of fatty livers in each group. Our method enables simultaneous estimation of liver fat content and tissue oxygenation, by multicomponent analysis with the curve-fitting method using the spectra of purified standards. NIR spectroscopic analysis revealed that the TG content in the liver of 1- and 3-week-CDD rats significantly increased compared to that of normal rats (Fig. 5). However, there was no statistical difference in the TG content between 3- and 7-week-CDD rats, which apparently reached maximum value by day 21. Teramoto *et al.* reported that the fat content in the CDD-induced fatty liver increases to the maximum value by 2 or 4 weeks.[10] This result greatly encouraged our study. Interestingly, total Hb and oxidized Hb in the liver decreased as the TG content increased, and there were significant differences both in total Hb and oxidized Hb between the livers of 1- and 3-week-CDD rats. In contrast, no significant differences were observed in the estimated cytochrome redox state among the livers in any rat group. These results indicated that the homeostasis of mitochondrial oxygenation was maintained in the fatty livers despite microcirculatory disturbance and hypoxia, which is compatible with the clinical observation that human fatty livers produce almost no clinical symptoms without stress conditions. Moreover, intriguing information that suggested a mechanism of fatty liver injury was provided by NIR spectroscopic analysis after ischemia and reperfusion (Fig. 7). In normal livers, the relative changes of total Hb, oxidized Hb and deoxidized Hb after reperfusion were minimal and immediately recovered to the pre-ischemic level after 60 min of reperfusion. In contrast, these parameters showed more salient changes in fatty livers. The total Hb and deoxidized Hb contents in the livers of 3-week-CDD rats after reperfusion were highly elevated and remained at a high level during observation, whereas these parameters in 1-week-CDD rats gradually recovered to the pre-ischemic level. These findings indicate that congestion and hypoxia occurred in the livers after reperfusion in proportion to the grade of fatty change. In addition, estimation of the redox state of Cyt. aa_3 provided notable information for understanding the mechanism of fatty liver injury. The level of oxidized-Cyt. aa_3 and reduced-Cyt. aa_3 in the normal livers remained at an almost pre-ischemic level after ischemia reperfusion. In contrast, relative changes of oxidized-Cyt. aa_3 and reduced-Cyt. aa_3 in fatty livers after ischemia–reperfusion did not sufficiently return to the level of pre-ischemia, which may indicate a disorder of the mitochondrial respiratory chain system. These results demonstrate that although the homeostasis of the mitochondrial cytochrome redox state may be maintained in fatty livers under non-stressful conditions despite significant decreases in total Hb and oxidized Hb, mitochondrial functions are difficult to be maintained under stress.

Fatty liver can be classified histologically as micro- or macrovesicular according to the size of the lipid vacuoles. Hepatic microvesicular steatosis is defined as cell enlargement that results from the cytoplasmic accumulation of small lipid vesicles. This is observed in several genetic or acquired conditions such as fatty liver of pregnancy, Reye's syndrome, and hepatotoxic reactions to drugs and toxins, which are related to impairment of mitochondrial β-oxidation.[33–36] On the other hand, hepatic macrovesicular steatosis is defined as hepatocyte distension that results from a single vacuole displacing the nucleus. This is the most common histological pattern in TG-related steatosis by chronic alcohol consumption, obesity, total parenteral nutrition and diabetes mellitus.[37–39] In the present study, fatty livers were induced by CDD, and the liver specimens from rats showed fatty infiltration, which was predominantly macrovesicular (Fig. 3). Despite these histological differences, the occurrence of microcirculatory disturbance is the most important factor that characterizes the viabil-

ity of fatty livers.[5,9,40] In this regard, our NIR spectroscopic technique can be considered one of the most useful tools to assess the accurate hepatic microcirculation in real time and may also provide predictive information regarding the viability of fatty liver.

For our *in vivo* experiments, we performed a laparotomy for NIR spectroscopic estimation to obtain pure spectra directly from liver without the interface of spectra from the abdominal wall. Although the NIR spectroscopic measurement is non-invasive to liver tissue, we had to perform a laparotomy to estimate hepatic fat content to avoid the intervention of fat contained in the abdominal wall. Therefore, at this stage, NIR spectroscopic measurement for fatty liver is most feasible in surgical settings, especially in transplantation situations. In the near future, if we could develop a new endoscopic NIR spectroscopic device, we may have another option to measure human fatty liver via the stomach.

In conclusion, we found a significant correlation between intrahepatic TG volume evaluated by NIR spectroscopic measurements and histological morphometric assessment. Moreover, our NIR spectroscopic measurement simultaneously evaluated Hb oxygenation in fatty liver, and provided predictive information for the viability of fatty livers.

ACKNOWLEDGMENT

THIS RESEARCH WAS supported in part by a Grant-in-Aid for Scientific Research (no. 21791289) of the Japan Society for the Promotion of Science.

REFERENCES

1 D'Alessandro AM, Kalayoglu M, Sollinger HW *et al.* The predictive value of donor liver biopsies for the development of primary nonfunction after orthotopic liver transplantation. *Transplantation* 1991; **51**: 157–63.
2 Todo S, Demetris AJ, Makowka L *et al.* Primary nonfunction of hepatic allografts with preexisting fatty infiltration. *Transplantation* 1989; **47**: 903–5.
3 Adam R, Reynes M, Johann M *et al.* The outcome of steatotic grafts in liver transplantation. *Transplant Proc* 1991; **23**: 1538–40.
4 Teramoto K, Bowers JL, Kruskal JB, Clouse ME. Hepatic microcirculatory changes after reperfusion in fatty and normal liver transplantation in the rat. *Transplantation* 1993; **56**: 1076–82.
5 Seifalian AM, Piasecki C, Agarwal A, Davidson BR. The effect of graded steatosis on flow in the hepatic parenchymal microcirculation. *Transplantation* 1999; **68**: 780–4.
6 Hui AM, Kawasaki S, Makuuchi M, Nakayama J, Ikegami T, Miyagawa S. Liver injury following normothermic ischemia in steatotic rat liver. *Hepatology* 1994; **20**: 1287–93.
7 Fukumori T, Ohkohchi N, Tsukamoto S, Satomi S. The mechanism of injury in a steatotic liver graft during cold preservation. *Transplantation* 1999; **67**: 195–200.
8 Ijaz S, Yang W, Winslet MC, Seifalian AM. Impairment of hepatic microcirculation in fatty liver. *Microcirculation* 2003; **10**: 447–56.
9 Fishbein TM, Fiel MI, Emre S *et al.* Use of livers with microvesicular fat safely expands the donor pool. *Transplantation* 1997; **64**: 248–51.
10 Teramoto K, Bowers JL, Khettry U, Palombo JD, Clouse ME. A rat fatty liver transplant model. *Transplantation* 1993; **55**: 737–41.
11 Markin RS, Wisecarver JL, Radio SJ *et al.* Frozen section evaluation of donor livers before transplantation. *Transplantation* 1993; **56**: 1403–9.
12 Franzen LE, Ekstedt M, Kechagias S, Bodin L. Semiquantitative evaluation overestimates the degree of steatosis in liver biopsies: a comparison to stereological point counting. *Mod Pathol* 2005; **18**: 912–6.
13 Thomsen C, Becker U, Winkler K, Christoffersen P, Jensen M, Henriksen O. Quantification of liver fat using magnetic resonance spectroscopy. *Magn Reson Imaging* 1994; **12**: 487–95.
14 Petersen KF, West AB, Reuben A, Rothman DL, Shulman GI. Noninvasive assessment of hepatic triglyceride content in humans with 13C nuclear magnetic resonance spectroscopy. *Hepatology* 1996; **24**: 114–7.
15 Szczepaniak LS, Babcock EE, Schick F *et al.* Measurement of intracellular triglyceride stores by H spectroscopy: validation in vivo. *Am J Physiol* 1999; **276**: E977–89.
16 Jobsis FF. Noninvasive, infrared monitoring of cerebral and myocardial oxygen sufficiency and circulatory parameters. *Science* 1977; **198**: 1264–7.
17 Leff DR, Orihuela-Espina F, Athanasiou T *et al.* "Circadian cortical compensation": a longitudinal study of brain function during technical and cognitive skills in acutely sleep-deprived surgical residents. *Ann Surg* 2010; **252**: 1082–90.
18 Wyatt JS, Cope M, Delpy DT, Wray S, Reynolds EO. Quantification of cerebral oxygenation and haemodynamics in sick newborn infants by near infrared spectrophotometry. *Lancet* 1986; **2**: 1063–6.
19 Hampson NB, Piantadosi CA. Near-infrared optical responses in feline brain and skeletal muscle tissues during respiratory acid-base imbalance. *Brain Res* 1990; **519**: 249–54.
20 Simonson SG, Piantadosi CA. Near-infrared spectroscopy. Clinical applications. *Crit Care Clin* 1996; **12**: 1019–29.
21 Noriyuki T, Ohdan H, Yoshioka S, Miyata Y, Asahara T, Dohi K. Near-infrared spectroscopic method for assessing the tissue oxygenation state of living lung. *Am J Respir Crit Care Med* 1997; **156**: 1656–61.

22 Asahara T, Dohi K, Sugino K *et al.* Living related partial liver transplantation for primary biliary cirrhosis – a case report. *Hiroshima J Med Sci* 1998; **47**: 31–7.
23 Ohdan H, Fukuda Y, Suzuki S, Amemiya H, Dohi K. Simultaneous evaluation of nitric oxide synthesis and tissue oxygenation in rat liver allograft rejection using near-infrared spectroscopy. *Transplantation* 1995; **60**: 530–5.
24 Tashiro H, Suzuki S, Kanashiro M *et al.* A new method for determining graft function after liver transplantation by near-infrared spectroscopy. *Transplantation* 1993; **56**: 1261–3.
25 Shibata S, Ohdan H, Noriyuki T, Yoshioka S, Asahara T, Dohi K. Novel assessment of acute lung injury by in vivo near-infrared spectroscopy. *Am J Respir Crit Care Med* 1999; **160**: 317–23.
26 Albanell E, Caceres P, Caja G, Molina E, Gargouri A. Determination of fat, protein, and total solids in ovine milk by near-infrared spectroscopy. *J AOAC Int* 1999; **82**: 753–8.
27 Neumeister V, Henker J, Kaltenborn G, Sprossig C, Jaross W. Simultaneous determination of fecal fat, nitrogen, and water by near-infrared reflectance spectroscopy. *J Pediatr Gastroenterol Nutr* 1997; **25**: 388–93.
28 Hilden M, Christoffersen P, Juhl E, Dalgaard JB. Liver histology in a "normal" population–examinations of 503 consecutive fatal traffic casualties. *Scand J Gastroenterol* 1977; **12**: 593–7.
29 Ground KE. Liver pathology in aircrew. *Aviat Space Environ Med* 1982; **53**: 14–8.
30 Underwood Ground KE. Prevalence of fatty liver in healthy male adults accidentally killed. *Aviat Space Environ Med* 1984; **55**: 59–61.
31 McCormack L, Petrowsky H, Jochum W, Mullhaupt B, Weber M, Clavien PA. Use of severely steatotic grafts in liver transplantation: a matched case-control study. *Ann Surg* 2007; **246**: 940–6; discussion 6–8.
32 Kitai T, Beauvoit B, Chance B. Optical determination of fatty change of the graft liver with near-infrared time-resolved spectroscopy. *Transplantation* 1996; **62**: 642–7.
33 Burt AD, Mutton A, Day CP. Diagnosis and interpretation of steatosis and steatohepatitis. *Semin Diagn Pathol* 1998; **15**: 246–58.
34 Hautekeete ML, Degott C, Benhamou JP. Microvesicular steatosis of the liver. *Acta Clin Belg* 1990; **45**: 311–26.
35 Fromenty B, Pessayre D. Impaired mitochondrial function in microvesicular steatosis. Effects of drugs, ethanol, hormones and cytokines. *J Hepatol* 1997; **26** (Suppl 2): 43–53.
36 Fromenty B, Berson A, Pessayre D. Microvesicular steatosis and steatohepatitis: role of mitochondrial dysfunction and lipid peroxidation. *J Hepatol* 1997; **26** (Suppl 1): 13–22.
37 Quigley EM, Marsh MN, Shaffer JL, Markin RS. Hepatobiliary complications of total parenteral nutrition. *Gastroenterology* 1993; **104**: 286–301.
38 Clain DJ, Lefkowitch JH. Fatty liver disease in morbid obesity. *Gastroenterol Clin North Am* 1987; **16**: 239–52.
39 Van Steenbergen W, Lanckmans S. Liver disturbances in obesity and diabetes mellitus. *Int J Obes Relat Metab Disord* 1995; **19** (Suppl 3): S27–36.
40 Takahashi K, Hakamada K, Totsuka E, Umehara Y, Sasaki M. Warm ischemia and reperfusion injury in diet-induced canine fatty livers. *Transplantation* 2000; **69**: 2028–34.

ORIGINAL ARTICLE

Rho-Kinase Inhibitor Targeting the Liver Prevents Ischemia/Reperfusion Injury in the Steatotic Liver Without Major Systemic Adversity in Rats

Shintaro Kuroda,[1] Hirotaka Tashiro,[1] Yasuhiro Kimura,[2] Kaori Hirata,[2] Misaki Tsutada,[2] Yoshihiro Mikuriya,[1] Tsuyoshi Kobayashi,[1] Hironobu Amano,[1] Yuka Tanaka,[1] and Hideki Ohdan[1]

[1]Department of Gastroenterological and Transplant Surgery, Applied Life Sciences, Institute of Biomedical & Health Sciences, Hiroshima University, Hiroshima, Japan; and [2]Department of Pharmaceutical Services, Hiroshima University Hospital, Hiroshima, Japan

Rho-kinase (ROCK) inhibitors improve liver blood flow after ischemia/reperfusion (IR) injury, especially in the setting of steatosis, by decreasing the resistance of intrahepatic microcirculation through hepatic stellate cell (HSC) relaxation. However, the systemic administration of ROCK inhibitors causes severe hypotension; therefore, liver-specific ROCK inhibition is required. Here, we tested vitamin A (VA)–coupled liposomes carrying the ROCK inhibitor Y-27632 for targeted HSCs in steatotic rats. Rat livers with steatosis induced by a choline-deficient diet were subjected to IR injury. The delivery site and effect of the ROCK inhibitor were investigated. After liposomal Y-27632 injection, the survival rate after IR, the liver blood flow, the portal perfused pressure, and the hemodynamics were investigated. Immunohistochemical studies showed VA–coupled liposome accumulation in livers. Liposomal Y-27632 was 100-fold more effective in inhibiting HSC activation than free Y-27632. Liposomal Y-27632 improved the survival rate after IR injury, the liver blood flow, and the portal perfusion pressure without severe hypotension. In contrast, untargeted Y-27632 elicited severe systemic hypotension. We conclude that VA–coupled liposomes carrying the ROCK inhibitor yield enhanced drug accumulation in the liver and thus mitigate IR injury in the steatotic liver and reduce major systemic adversity. ***Liver Transpl 21:123-131, 2015.*** **© 2014 AASLD.**

Received June 10, 2014; accepted October 4, 2014.

Liver steatosis increases the risk of postoperative morbidity and mortality after liver surgery, including liver transplantation.[1-3] Ischemia/reperfusion (IR) injury is one of the most critical complications commonly associated with liver surgery.[4,5] Compared with healthy livers, steatotic livers are vulnerable to IR.

Hepatic stellate cells (HSCs) are located in the space of Disse surrounding sinusoidal endothelial cells (SECs). HSCs are thought to play a role in modulating intrahepatic vascular resistance because of their capacity to contract through a Rho signaling mechanism. HSCs undergo contraction or relaxation in

Additional Supporting Information may be found in the online version of this article.

Abbreviations: AST, aspartate aminotransferase; empty Lip, liposome with no drug; empty VA-Lip, vitamin A–coupled liposome with no drug; GFP, green fluorescence protein; HSC, hepatic stellate cell; IR, ischemia/reperfusion; Lip-GFP, liposome carrying green fluorescence protein; Lip-Y, liposome carrying Y-27632; MAP, mean arterial pressure; MLC, myosin light chain; P-MLC, phosphorylated myosin light chain; ROCK, Rho-kinase; SD, standard deviation; SEC, sinusoidal endothelial cell; VA, vitamin A; VA-Lip-GFP, vitamin A–coupled liposome carrying green fluorescence protein; VA-Lip-Y, vitamin A–coupled liposome carrying Y-27632.

Potential conflict of interest: Nothing to report.

This work was supported in part by the Japan Society for the Promotion of Science (Grant-in-Aid for Scientific Research 21591748 to Hirotaka Tashiro). This work was carried out in part at the Analysis Center of Life Science in Hiroshima University.

Address reprint requests to Hirotaka Tashiro, M.D., Ph.D., Department of Gastroenterological and Transplant Surgery, Applied Life Sciences, Institute of Biomedical & Health Sciences, Hiroshima University, 1-2-3 Kasumi, Hiroshima 734-8551, Japan. Telephone: 81 82 257 5222; FAX: 81 82 257 5224; E-mail: htashiro@hiroshima-u.ac.jp

DOI 10.1002/lt.24020
View this article online at wileyonlinelibrary.com.
LIVER TRANSPLANTATION.DOI 10.1002/lt. *Published on behalf of the American Association for the Study of Liver Diseases*

response to certain stimuli and, consequently, regulate the microcirculation by increasing or decreasing the diameter of the sinusoidal lumen.[6] Rho-kinase (ROCK) is a key player in HSC contraction and is activated by active Rho A, a small guanosine triphosphatase coupled with many vasoconstrictor receptors such as endothelin that are involved in regulating portal hypertension.[7-12] The inhibition of intrahepatic ROCK by Y-27632 attenuates resistance in cirrhotic rats, as shown by in situ liver perfusions.[7,12,13]

In our previous study, activation of Rho-ROCK signaling increased HSC susceptibility in rat steatotic livers to IR injury, and this indicated that HSC activation in the steatotic liver is associated with ROCK2 up-regulation and that enhanced ROCK2 activation is involved in the induction of IR injury in steatotic livers. Additionally, we found that an intra-abdominal infusion of fasudil, a specific ROCK inhibitor, significantly alleviated IR injury in steatotic livers.[14] However, ROCK inhibitors have been reported to lead to several detrimental adverse effects, such as hypotension and ileus, via the inhibition of migration, contraction, adherence, and division of systemic cells of various organs.[15,16] To avoid these adverse effects, a more selective drug delivery system for HSCs is required. Recently, a new drug delivery system using liposomes that target HSCs has been reported. Vitamin A (VA)-coupled liposomes preferentially target HSCs, which have a remarkable capacity for VA uptake, most likely through receptors for retinol-binding protein.[17]

In this study, we tried to deliver an encapsulated ROCK inhibitor in VA-coupled liposomes to the liver in order to reduce hepatic IR injury on the basis of a study by Sato et al.[17] We also examined whether this new drug reduced any detrimental adverse effects of the ROCK inhibitor (eg, hypotension).

MATERIALS AND METHODS

Animals

Four-week-old male Wistar rats were purchased from Charles River Breeding Laboratories (Osaka, Japan). The rats were fed either a choline-deficient diet (Hiroshima Institute for Experimental Animals, Hiroshima, Japan) for 6 weeks to encourage the development of steatosis in the liver or a normal diet that caused normal liver development. All animal experiments were performed according to the guidelines set by the US National Institutes of Health (1985). This experimental protocol was approved by the ethics review committee for animal experimentation of the Graduate School of Biomedical Sciences at Hiroshima University.

Liver IR

The rats were placed under anesthesia, and whole rat livers were subjected to warm ischemia via the clamping of the hepatic artery and the portal vein with microvascular clips. The specific ROCK inhibitor (Y-27632, Wako, Osaka, Japan) or a liposomal drug for Y-27632 was used to investigate the effect of ROCK inhibition on liver IR injury. The selected rats were pretreated with different quantities of drugs (via an intravenous bolus injection) 30 minutes before the induction of ischemia.

Preparation of VA-Coupled Liposomes Carrying the ROCK Inhibitor

Three types of empty liposomes (Coatsome EL-C-01, EL-N-01, and EL-A-01; NOF Corp., Tokyo, Japan), were used to deliver Y-27632. VA-coupled liposomes carrying the ROCK inhibitor were prepared as previously described with some modifications.[17,18] Briefly, 25 mg of the empty liposome product was added to 400 μL of a Y-27632 solution [20 mg/mL; liposome carrying Y-27632 (Lip-Y)]. To prepare VA-coupled liposomes, 200 nmol of VA (retinol; Sigma-Aldrich, St. Louis, MO) dissolved in dimethyl sulfoxide was mixed with the liposome suspensions (100 nmol as liposome) via vortexing in a 1.5-mL tube at 25°C [vitamin A–coupled liposome carrying Y-27632 (VA-Lip-Y)]. The quantities of Y-27632 taken up by the liposome were determined with a high-performance liquid chromatography system (LC-2010A; Shimadzu, Kyoto, Japan; Fig. 1A-C). Any free VA or Y-27632 that was not taken up by liposomes was separated from the liposomal preparations with a micropartition system (Vivaspin 2 concentrator; molecular weight cutoff = 30,000; polyethersulfone; Vivascience, Sigma-Aldrich, St. Louis, MO). The liposomal suspension was added to the filters and centrifuged 3 times at 1500*g* for 5 minutes each at 25°C. Fractions were collected, and the material trapped in the filter was reconstituted with phosphate-buffered saline to achieve the desired dose for in vitro or in vivo use. For the Lip-Y and VA-Lip-Y control groups for each experiment, we used liposomes without Y-27632 (empty Lip) or VA-coupled liposomes without Y-27632 (empty VA-Lip).

Isolation of HSCs

HSCs were isolated from rat steatotic livers according to previously described procedures.[14,19,20] Purity was estimated with ordinal light and fluorescence microscopy examinations and via indirect enzyme immunoreactivity with an anti-desmin antibody (Dako, Versailles, France). HSCs were grown in standard tissue culture plastic flasks in Dulbecco's minimum essential medium with 10% fetal bovine serum and antibiotics.

Collagen Gel Contraction Assay

The contractility of HSCs was evaluated with hydrated collagen gel lattices on 24-well culture plates as described previously with some modifications.[14,19,21]

Immunofluorescence of HSCs and Tissue Sections

To assess the activation of HSCs, phalloidin staining of isolated HSCs was performed according to previously

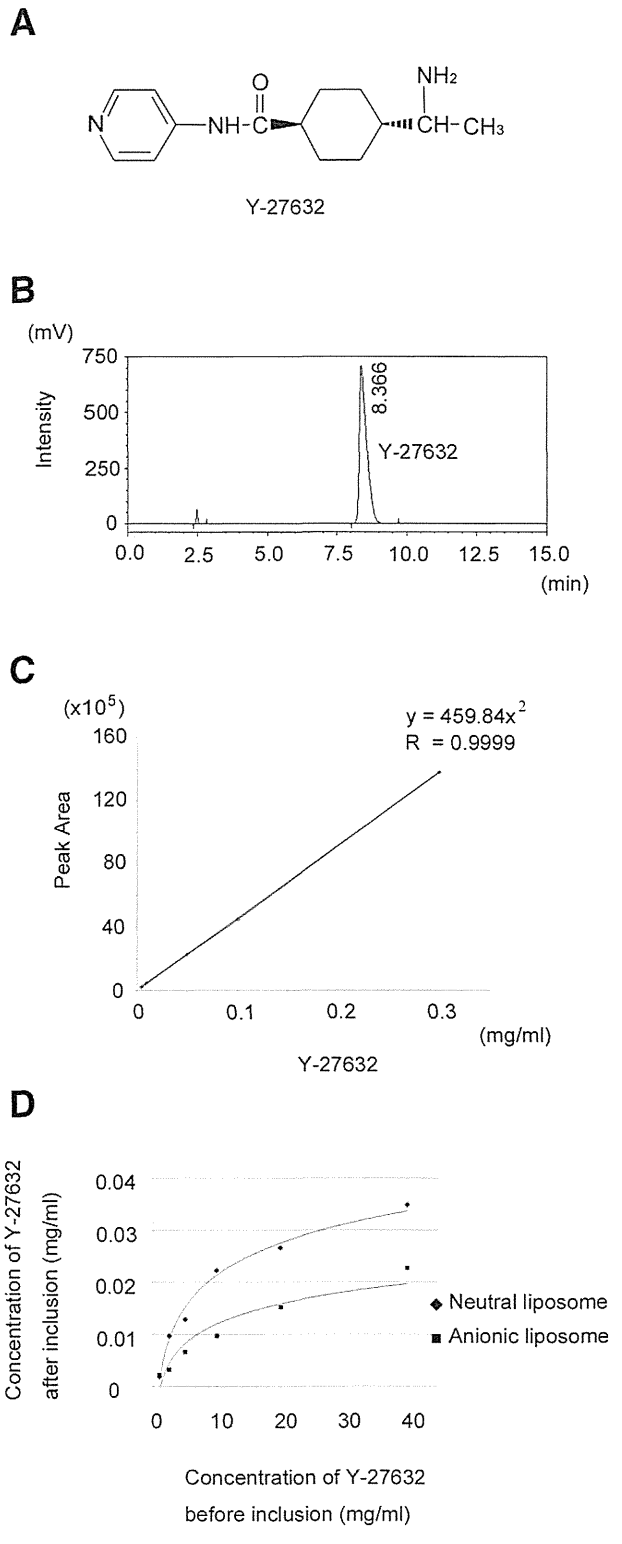

Figure 1. Preparation of VA-coupled liposomes carrying the ROCK inhibitor. (A) Chemical structure of Y-27632. (B) Chromatogram of Y-27632 extracted from VA-Lip-Y or Lip-Y. The specific peak of Y-27632 was identified at approximately 8.4 minutes. (C) Calibration curve for the determination of coupled Y-27632 in the liposome. (D) Comparison of the ratio of inclusion of Y-27632 among the 3 liposomes. The ratio of inclusion of Y-27632 was highest for the neutral liposome. Y-27632 was almost not included in the cationic liposome (data not shown).

described procedures.[14,22] Samples were observed under a conventional fluorescence microscope (BZ-9000; Keyence, Osaka, Japan). The average brightness of the 5 random areas was measured by microscopy (×400) with BZ-H1C dynamic cell count software (Keyence). For the histological analysis, liver specimens were collected from the middle hepatic lobe. To assess the accumulation of green fluorescence protein (GFP), frozen sections of the liver, lungs, heart, kidneys, and spleen were observed. To identify HSCs in the frozen liver sections, desmin staining was performed. The specific antibody against desmin was purchased from Abcam (Tokyo, Japan).

Statistical Analysis

Survival rates were compared with the Kaplan-Meier method and analyzed with the log-rank test. Other data are expressed as average values and standard deviations (SDs). Statistical analyses of experimental groups were performed with the *t* test. A 1-way analysis of variance was used for multiple comparisons. $P < 0.05$ was considered statistically significant. Statistical analyses were performed with SPSS 16 (SPSS Japan, Inc., Tokyo, Japan). For other descriptions of the materials and methods used in this study, please see the supporting information.

RESULTS

Preparation of VA-Coupled Liposomes Carrying the ROCK Inhibitor

We examined the inclusion of Y-27632 in 3 empty liposome products with high-performance liquid chromatography system: Coatsome EL-C-01 as a cationic liposome, EL-N-01 as a neutral liposome, and EL-A-01 as an anionic liposome. The ratio of Y-27632 inclusion was highest with the neutral liposome. The concentration of included Y-27632 increased in a dose-dependent manner and plateaued at a concentration of approximately 40 mg/mL (Fig. 1D). We used this concentration for subsequent experiments.

Y-27632 Suppresses the Level of Phosphorylation of Myosin Light Chains (MLCs) in HSCs

ROCK mediates cytoskeleton-dependent cell functions by enhancing MLC phosphorylation. We examined whether the ROCK inhibitor Y-27632 suppresses the phosphorylation level of MLCs in HSCs. Y-27632–treated HSCs showed dose-dependent suppression of the phosphorylation level of MLCs, with almost complete suppression at 10 μM (Fig. 2A).

Contractility of HSCs Isolated From Steatotic Rat Livers

To evaluate the effectiveness of VA-Lip-Y with respect to contractility, HSCs isolated from rat steatotic livers were cultured on hydrated collagen gels. Contraction

was measured by the reduction in the initial area of the gel. In the control group, the areas of the gels with HSCs were significantly lower than the areas of the gels without HSCs (data not shown). Empty Lip and empty VA-Lip as controls for Lip-Y and VA-Lip-Y did not effectively suppress these changes. In the presence of Y-27632 (10 μM), a reduction was not observed in the gel area with HSCs ($P < 0.01$). Similarly, a reduction in the area was not observed ($P < 0.01$) in the presence of Lip-Y (0.1 μM) or VA-Lip-Y (0.1 μM; Fig. 2B,C).

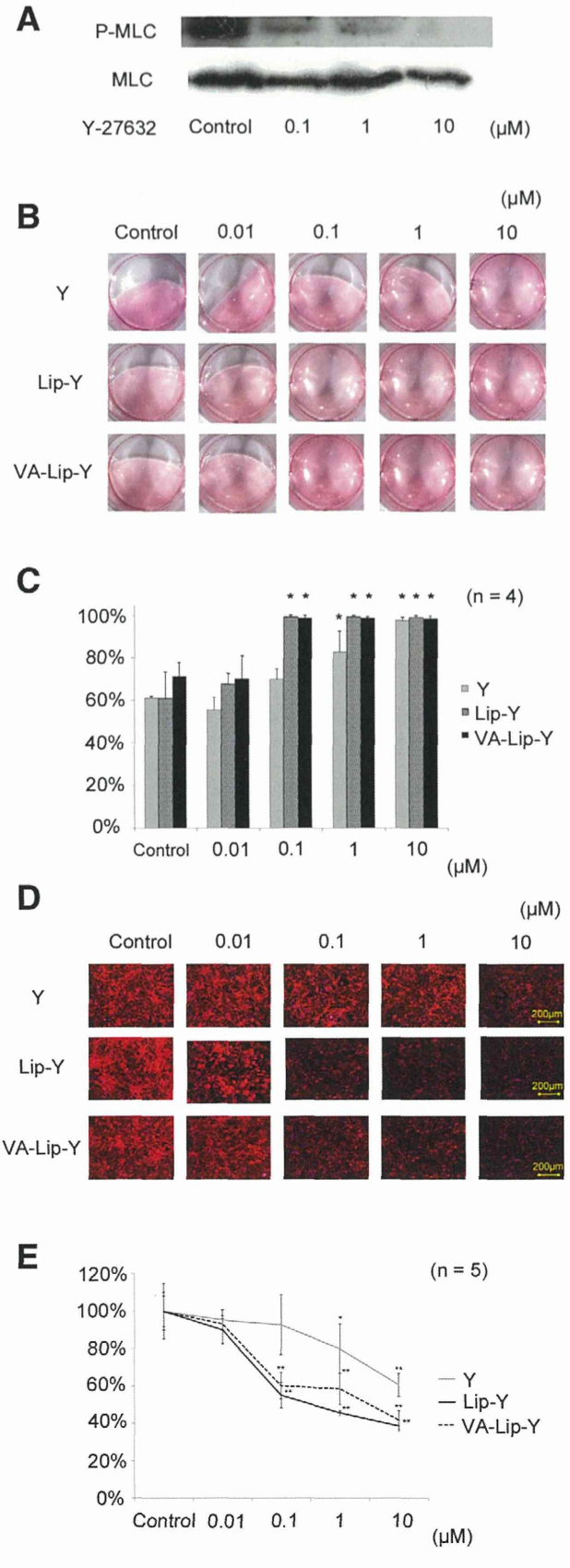

Figure 2. Effectiveness of VA-Lip-Y for activated HSCs in vitro. (A) Western blot analysis of the phosphorylation of MLCs in HSCs. The Y-27632 dose-dependently suppressed the phosphorylation level of MLCs in HSCs. (B) Collagen gel contraction assay. The contraction of collagen gels was induced by the activation of isolated HSCs that were untreated (control) or were treated with Y-27632, Lip-Y, or VA-Lip-Y. Without the addition of HSCs, the collagen gels did not contract during the observation period (not shown). (C) Changes in the collagen gel area induced by the contraction of HSCs. Average values (and SDs) of 4 independent experiments are shown. *$P < 0.01$ versus each control. (D) F-actin expression in isolated HSCs. HSCs were treated with Y-27632, Lip-Y, or VA-Lip-Y (24 hours). The cells were stained to show F-actin (red) and nuclei (blue). The control showed many stress fibers and high F-actin expression. In contrast, HSCs treated with Y-27632, Lip-Y, or VA-Lip-Y dose-dependently suppressed stress fiber formation and F-actin expression. (E) Levels of F-actin expression on HSCs. Average values (and SDs) of 5 independent experiments are shown. *$P < 0.05$ and **$P < 0.01$ versus each control. Y indicates Y-27632.

Effectiveness of VA-Lip-Y With Respect to the Morphological Features of HSCs

HSCs isolated from rat steatotic livers showed increased stress fiber formation and F-actin expression 24 hours after culture. The empty VA-Lip control for VA-Lip-Y and the empty Lip control for Lip-Y did not suppress the observed changes (Supporting Fig. 1). HSC stress fiber formation and F-actin expression were significantly suppressed by 0.1 μM VA-Lip-Y and Lip-Y ($P < 0.01$). In contrast, HSC activation was not suppressed by the same concentration of Y-27632 but was significantly suppressed at 10 μM ($P < 0.01$; Fig. 2D,E). Next, to confirm the toxicity of liposomes to HSCs, we examined the morphological changes of HSCs with time after the administration of VA-Lip-Y (Supporting Fig. 2). After administration, HSC stress fiber formation and F-actin expression were suppressed and gradually reactivated within 48 hours.

Delivery of GFP to the Liver by Liposomes

A histological analysis showed that GFP accumulation in the steatotic liver specimens injected with the vitamin A–coupled liposome carrying green fluorescence protein (VA-Lip-GFP) was significantly higher than that with the liposome carrying green fluorescence protein (Lip-GFP; $P < 0.01$; Fig. 3A,B). Additionally, there was no evidence of GFP accumulation in the heart, lungs, kidneys, or small intestine. Although there was slight GFP accumulation in the spleen, which was likely caused by nonspecific uptake by macrophages (Fig. 3C,D), GFP accumulation was

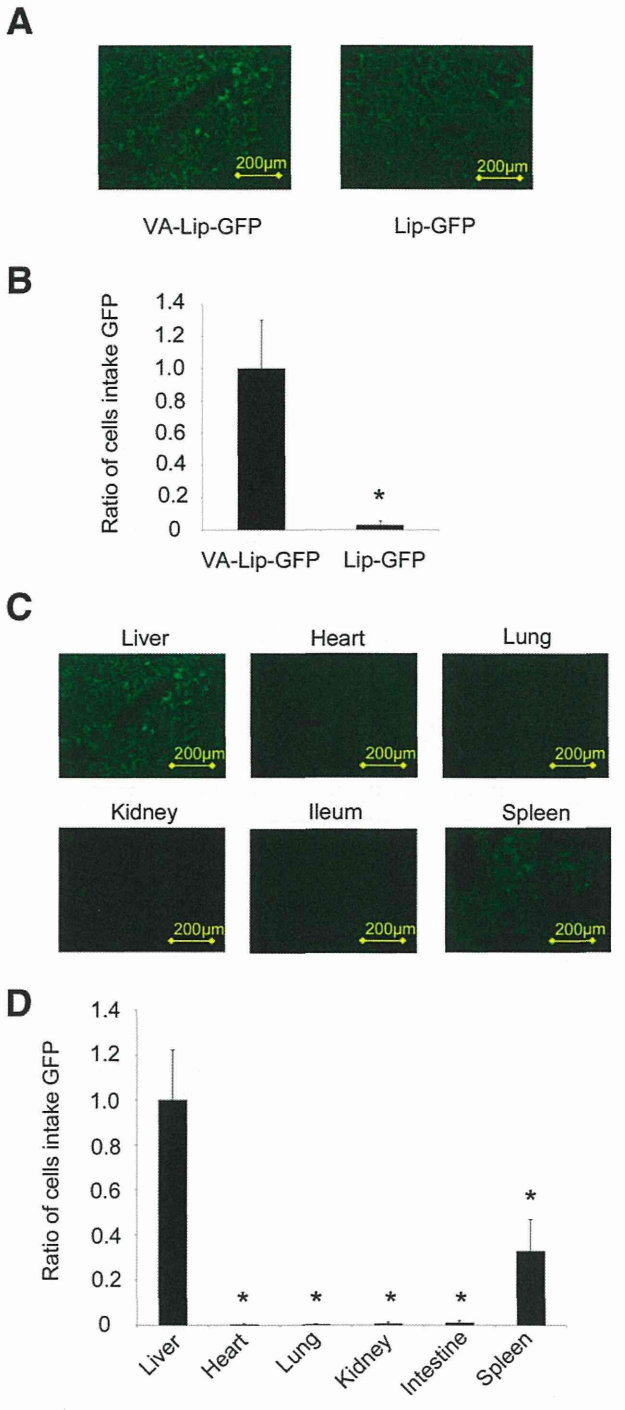

Figure 3. Liposome accumulation in steatotic livers. (A) Liver tissue sections of rats with steatotic livers treated with Lip-GFP or VA-Lip-GFP. (B) Ratio of the cell intake of GFP in liver tissue sections treated with VA-Lip-GFP to that in sections treated with Lip-GFP. (C) Tissue sections of each organ treated with VA-Lip-GFP. Liver, heart, lung, kidney, small intestine, and spleen sections were observed under a conventional fluorescence microscope. (D) Ratio of the cell intake of GFP in liver tissue sections versus other organs. Average values (and SDs) for individual groups are shown (n = 5 for all groups). *$P < 0.01$ versus the control group.

significantly enhanced in the steatotic liver versus the spleen ($P < 0.01$). GFP accumulation was also enhanced in the normal liver. Furthermore, GFP accumulation in normal liver tissue sections included the desmin-stained area (Fig. 4A,B).

VA-Lip-Y Protects Steatotic Livers against IR Injury

We examined the effect of Y-27632 on the survival of rats with steatotic livers after 45 minutes of hepatic ischemia. None of the 10 untreated rats with steatotic livers survived more than 4 days. The survival rate of rats with steatotic livers was not improved by Y-27632 (0.1 mg/kg); the 1-week survival rate was 20% (2/10 rats). However, the survival of rats with steatotic livers was significantly prolonged by Y-27632 (10 mg/kg), Lip-Y (0.1 mg/kg), and VA-Lip-Y treatment (0.1 mg/kg); the 1-week survival rates were 60% (6/10 rats), 60% (6/10 rats), and 70% (7/10 rats), respectively ($P < 0.05$, $P < 0.01$, and $P < 0.01$, respectively). The survival rates did not significantly differ for Y-27632 (10 mg/kg), VA-Lip-Y (0.1 mg/kg), and Lip-Y (0.1 mg/kg; Fig. 5A).

Serum aspartate aminotransferase (AST) levels and histological changes in steatotic livers were measured after 30 minutes of ischemia followed by 3 hours of reperfusion. Sinusoidal congestion and massive necrosis were observed in the steatotic livers from the control, whereas no significant necrosis was observed in steatotic livers from rats treated with VA-Lip-Y (0.1 mg/kg; Fig. 5B). The serum AST levels in rats treated with a 10 mg/kg injection of Y-27632 and a VA-Lip-Y injection (0.1 mg/kg) were significantly lower than those of the control and Y-27632 rats at the 0.1 mg/kg concentration ($P < 0.01$ and $P < 0.01$, respectively; Fig. 5C).

VA-Lip-Y Improves Hepatic Tissue Blood Flow in Steatotic Livers After IR

Liver blood flow was measured during drug injection, ischemia, and reperfusion. In untreated rats with steatotic livers, liver blood flow decreased after ischemia and did not recover after reperfusion. The liver blood flow for the empty VA-Lip-Y group was the same as that for untreated rats (Supporting Fig. 3). In the rats treated with Y-27632 at 10 mg/kg, the liver blood flow after ischemia was significantly less than that in untreated rats ($P < 0.05$). In contrast, blood flow recovered in the VA-Lip-Y (0.1 mg/kg)–treated rats after reperfusion; the blood flow 10 minutes after reperfusion was significantly higher than that in the untreated rats ($P < 0.05$), and the blood flow at 15 minutes after reperfusion was significantly higher than that in rats treated with 0.1 mg/kg Lip-Y ($P < 0.05$; Fig. 6A,B).

Next, to determine the influence of IR on microvascular blood flow in the hepatic lobule, the portal perfusion pressure was assessed in isolated rat steatotic livers. Perfusion pressures were measured after 45 minutes of total hepatic ischemia followed by 15 minutes of reperfusion. The portal perfusion pressures of rats after IR were significantly higher than those of rats that did not undergo IR ($P < 0.01$), and Y-

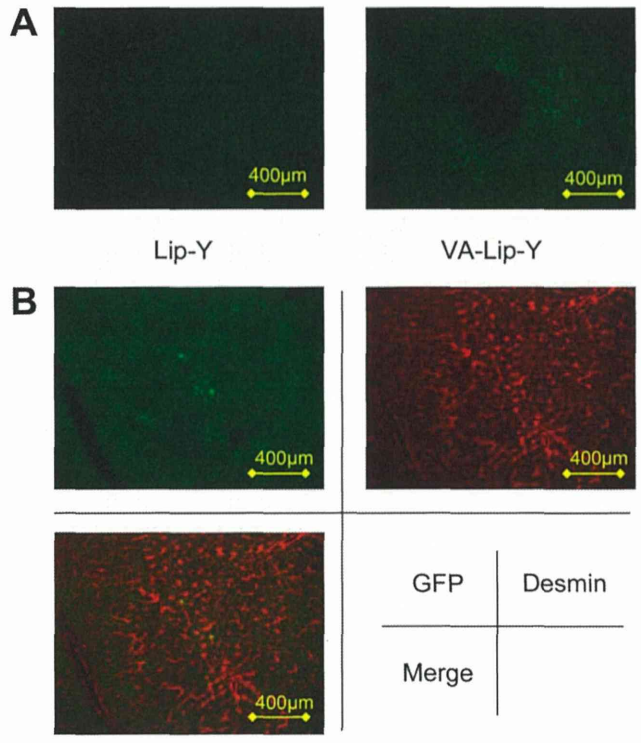

Figure 4. Accumulation of liposomes in liver tissue sections of rats with normal livers. (A) Liver tissue sections of rats treated with Lip-GFP or VA-Lip-GFP. (B) Desmin-stained liver tissue section of a rat treated with VA-Lip-GFP. The area showing an accumulation of GFP in the liver tissue section includes the desmin-stained area.

27632 did not decrease the portal perfusion pressure at the concentration of 0.1 mg/kg. However, the portal perfusion pressure was significantly suppressed 30 minutes before the pre-injection of Y-27632 at 10 mg/kg, Lip-Y at 0.1 mg/kg, and VA-Lip-Y at 0.1 mg/kg ($P<0.01$, $P<0.01$, and $P<0.01$, respectively). The portal perfusion pressures of the VA-Lip-Y group were significantly lower than those with Y-27632 at 10 mg/kg and Lip-Y at 0.1 mg/kg ($P<0.01$ and $P<0.01$, respectively; Fig. 6C).

Mean Arterial Pressure (MAP) Measurement in Rats During Drug Administration

To determine the effect of drug injection on blood pressure, the MAP of rats was measured during drug administration. The MAP of the rats that received bolus injections of VA-Lip-Y at a concentration of 0.1 mg/kg exhibited a decrease in MAP to 66.3 mm Hg, but the MAP in the VA-Lip-Y group was significantly higher than that for the Y-27632 (10 mg/kg) and Lip-Y groups. Subsequently, the MAP of the VA-Lip-Y group improved to 83.3 mm Hg ($P<0.01$ and $P<0.01$, respectively; Fig. 6D).

DISCUSSION

We have developed a new drug system for delivering a ROCK inhibitor encapsulated in VA-coupled liposomes

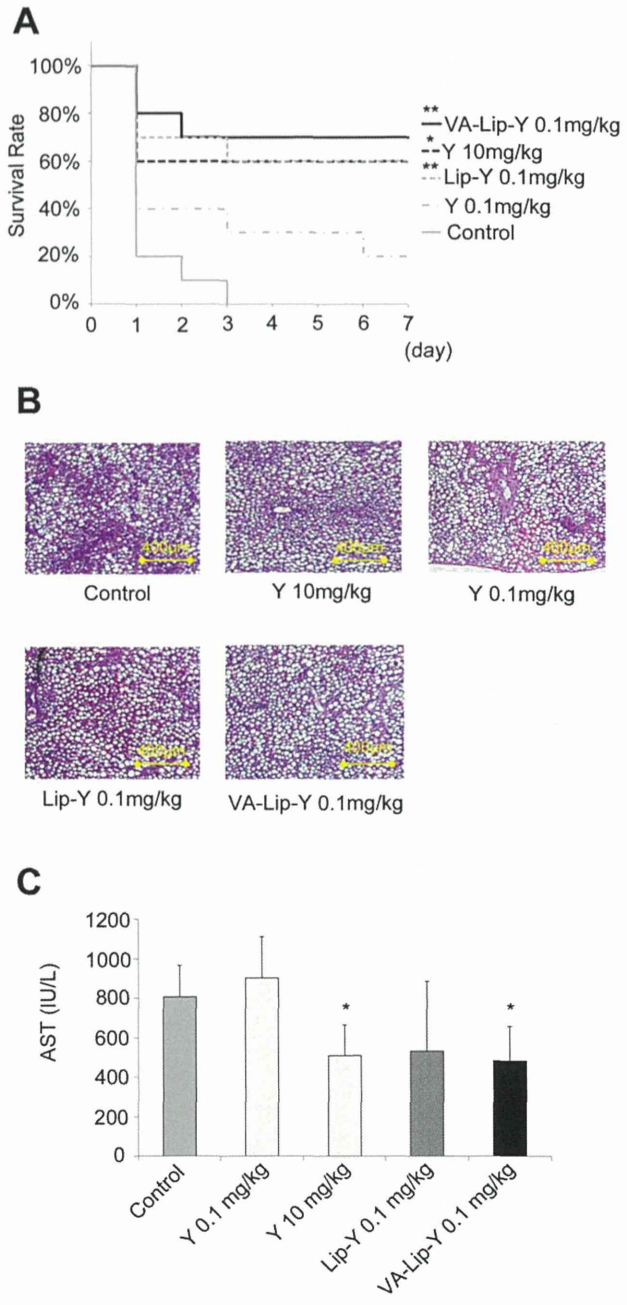

Figure 5. VA-Lip-Y protects steatotic livers against IR injury. Rats with steatotic livers were treated with IR. Each drug was administered 30 minutes before IR. (A) Survival rates of rats with steatotic livers after IR. The rats underwent 45 minutes of ischemia (n = 10). *$P<0.05$ and **$P<0.01$ versus the control group. (B) Histological examination of steatotic livers after IR. The rats underwent 30 minutes of ischemia followed by 3 hours of reperfusion (representative hematoxylin and eosin–stained liver sections). (C) Serum AST levels in rats with steatotic livers. The rats underwent 30 minutes of ischemia followed by 3 hours of reperfusion. Average values (and SDs) for individual groups are shown (n = 5 for all groups). *$P<0.05$ versus the control group. Y indicates Y-27632.

to the liver to ameliorate hepatic IR injury without the detrimental adverse effects of global ROCK inhibition (eg, hypotension). The current study shows that (1) VA-coupled liposomes carrying the ROCK inhibitor

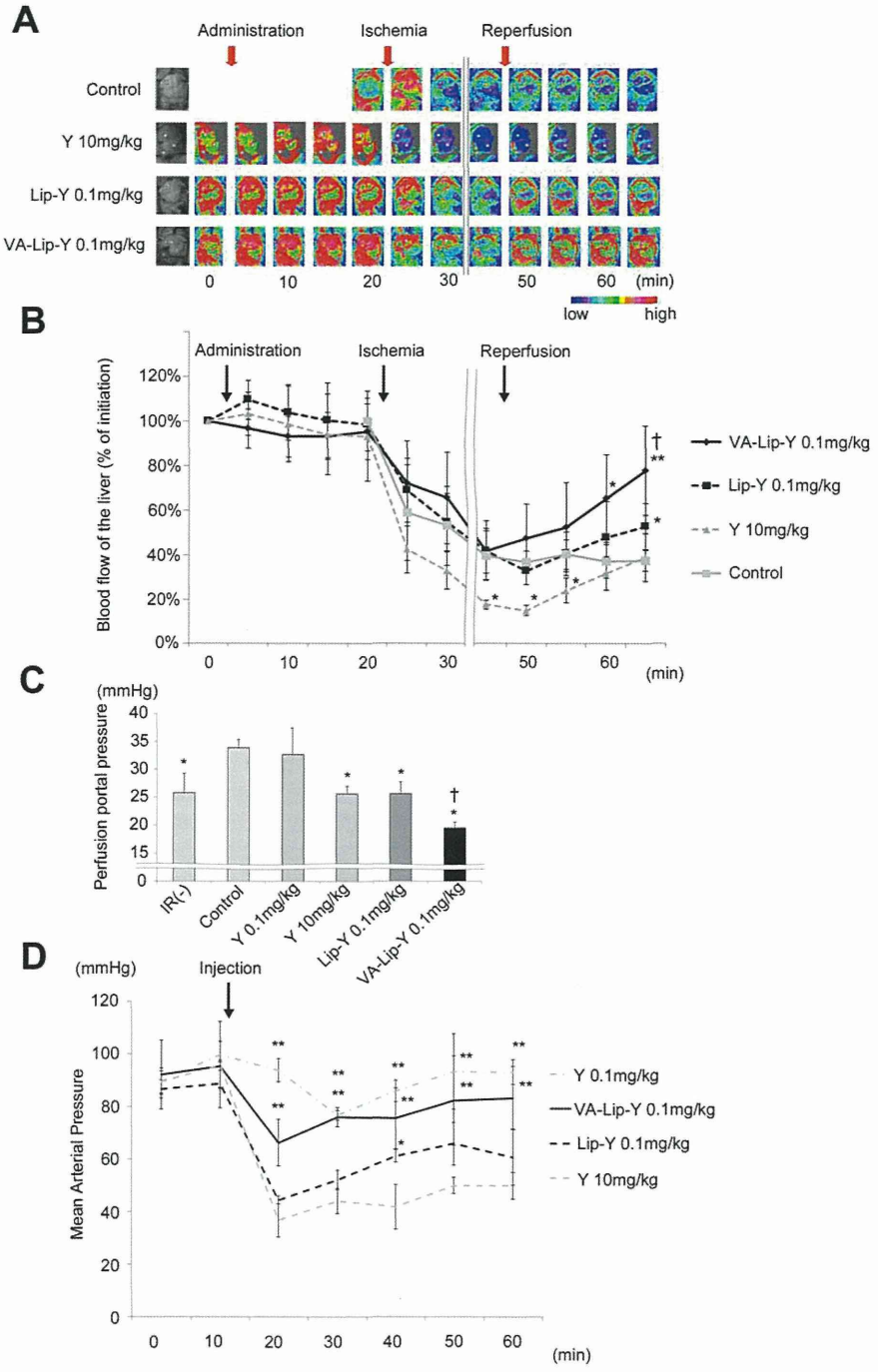

Figure 6. VA-Lip-Y improves the hepatic microcirculation after IR. (A) Change in the liver blood flow after IR. Pseudocolor images of the liver are shown; the color bar indicates blood flow. (B) Comparison of changes in the liver blood flow over time. Each drug was administered 15 minutes before ischemia. After 30 minutes of ischemia, the liver blood flow was measured for 15 minutes. Average values (and SDs) for individual groups are shown (n = 4 for all groups). *$P < 0.05$ and **$P < 0.01$ versus the control group; †$P < 0.05$ versus the Lip-Y group. (C) Portal pressures in isolated perfused livers. Livers were untreated, treated with 45 minutes of ischemia followed by 15 minutes of reperfusion, or pre-injected with each drug 30 minutes before IR. Average values (and SDs) for individual groups are shown (n = 5 for all groups). *$P < 0.01$ versus the control group; †$P < 0.05$ versus the Y-27632 (10 mg/kg) and Lip-Y groups (0.1 mg/kg). (D) MAP in rats. MAP was measured in rats during drug administration. Average values (and SDs) for individual groups are shown (n = 5 for all groups). *$P < 0.05$ and **$P < 0.01$ versus the Y-27632–treated group. Y indicates Y-27632.

were predominantly taken up into livers, (2) VA-coupled liposomes carrying the ROCK inhibitor were approximately 100-fold more effective in suppressing the contractility of the activated HSCs than the nonliposomal ROCK inhibitor, (3) VA-coupled liposomes carrying the ROCK inhibitor significantly protected steatotic livers against IR injury in comparison with the nonliposomal ROCK inhibitor, and